CHALMERS

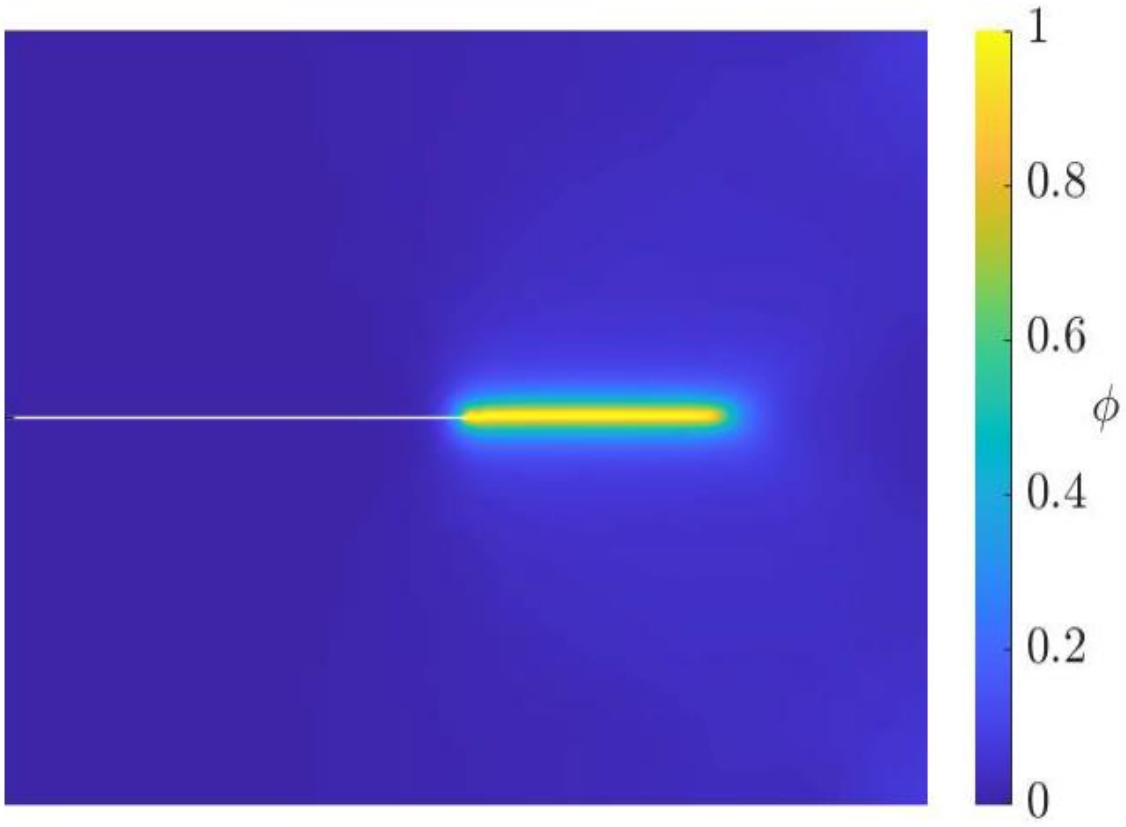

Studentarbeten – Mekanik och maritima vetenskaper (M2) – Projektarbeten

Phase-field modelling of fatigue crack propagation

TME131 Project in Applied Mechanics 2023

Sharvil Degwekar
Ankeet Mohan Purantagi
Afroditi Tzanetou
Gustav Zetterlund
Louise Åkesson

Department of Mechanics and Maritime Sciences
CHALMERS UNIVERSITY OF TECHNOLOGY
Göteborg, Sweden 2023

Phase-field modelling of fatigue crack propagation
TME131 Project in Applied Mechanics 2023

Studentarbeten – Mekanik och maritima vetenskaper (M2) – Projektarbete

Department of Mechanics and Maritime Sciences
Chalmers University of Technology
SE-412 96 Göteborg
Sweden
Telephone +46 (0)31 772 1000

Preface

The work in the present report was carried out as a part of the course TME131 Project in Applied Mechanics, which is a mandatory course within the Applied Mechanics Masters programme at Chalmers. The course was carried out during spring semester 2023.

The project was supervised by Fredrik Larsson, Ritukesh Bharali and Mohammad Salahi Nezhad.

Abstract

Fracture prediction and modeling are crucial in studying the behavior of materials under stress. This research focuses on utilizing the phase field method for accurate fracture prediction, which offers distinct advantages over traditional methods by representing fractures implicitly as smooth fields. The phase field method was implemented and analyzed using Matlab and COMSOL as tools, aiming to investigate and gain insights into the ease and feasibility of phase-field modelling for fatigue fracture problems. This was conducted mainly by introducing a fatigue degradation function, with the purpose of simulating the degrading process of the material after repeated cyclic loading. Through comprehensive analysis, quantities of interest such as the history variable, accumulated strain energy, and damage variable were examined. The obtained trends and results were found to align with existing literature, although neither calibration nor validation was conducted due to time limitations. Suggestions for future work include implementing a force-controlled load, calibration of the fatigue degradation function for a larger amount of load cycles, and validation with experimental data. Nevertheless, the results obtained from the fatigue implementation can provide a solid foundation for continued research. In conclusion, the progress during the project highlighted the potential of the phase-field model to predict fatigue fracture by modelling the crack through a damage field. Hence, fatigue prediction using phase-field modelling has the potential to make significant progress and thus contribute to less computationally expensive simulations for more complex fatigue fracture problems.

Keywords: phase field, fatigue, cyclic loading, fatigue degradation function

Contents

1 Introduction

When predicting the strength of a certain solid component one usually wants an overall mechanical response of the whole body. This can be performed by implementing a finite element analysis. However, in cases where the FE model includes fracture prediction the crack propagation can be extremely difficult and expensive to simulate using an explicit model. One method developed to circumvent this problem is phase-field modelling. The approach has proved good results for solving the development of cracks both in terms of crack nucleation and crack propagation without any need for an initial notch [6]. The phase-field approach is based on crack modelling in a smeared sense where material damage is represented by a damage variable ϕ in each node ranging from 0 to 1, where 0 indicates full material integrity and 1 material fracture. In other words, the discrete discontinuous phenomenon is by utilizing phase-modelling instead represented as a smooth function [7].

1.1 Background

Phase-field modelling of fractures has due to significant interest and research led to an established approach able to predict crack patterns and the overall mechanical response of structures. This is however mainly developed for cases with monotonic static loading or high-velocity dynamic fracture since the concept is relatively new [7]. Due to the many manufacturing processes and industrial applications involving oscillating loads of different kinds, models that can simulate crack propagation and fatigue fracture are of major importance for engineers and society in general. Furthermore, fatigue failure is one of the most frequently occurred types of failure in structures, and is less predictable than failure caused by exceeding the ultimate strength of the material [5]. Hence, due to its beneficial simulation features even in complex crack problems, the development of phase-field models for fatigue applications is of great interest amongst researchers and engineers [4].

1.2 Objective

This project aims at developing and evaluating a phase-field model for fatigue crack-growth problems. In addition to a brief literature study, the project will mainly consist of working toward the following goals:

- Develop and qualitatively calibrate constitutive models for phase-field evolution.
- Implement a finite element code based on phase-field modelling for elasticity.
- Implement fatigue loading to the phase-field model and compare with experiments in the literature.
- Qualitatively assess the feasibility and ease of the implementation when using phase-field fracture modeling for fatigue applications.

1.3 Scope

Since the project is being carried out during weeks 12 to 21, the time budget will be one of the major limitations. As a result, relevant boundaries for the project are introduced below. It is clear that these boundaries will affect the resulting model and its validity in real-life applications, especially the boundaries related to the modelling assumptions. Consequently, considering and acknowledging

them in the final conclusion is essential for the usage and further development of the model. As mentioned, the first two boundaries below consider the specific modelling assumptions while the last boundary is more general for the project itself.

- The simulations are limited to 2D (in-plane).
- Only elastic response coupled to phase-field damage (brittle fracture) is considered.
- Usage of the software is limited to available options on Chalmers' computers.

Due to the first two boundaries, the implemented 2D finite element model could be used for the prediction of the crack propagation in applications when the plane stress or plane strain assumption is valid. In practice, plane strain assumption finds more applications in engineering problems such as the prediction of the crack propagation in railway components.

2 Theory

In this chapter relevant theory for understanding of phase-field modelling of fatigue, is presented. First, theory on phase-field modelling is introduced along with its corresponding numerical counterpart. Thereafter the fatigue extension of the phase-field model is described.

2.1 Phase-field modeling

In this section, the strong form of the the phase-field model is derived as the equations that are used to solve the fracture problem under monotonic loading. Based on the strong form of the problem, the weak form of it is derived using Galerkin's method. Finally, the formulation of the FE approximation follows, describing the numerical method that is used to solve the problem in MATLAB.

2.1.1 Strong Form

The fracture process is governed by the minimization of the potential energy where the internal energy is expressed as a summation of the materials bulk energy and the dissipative fracture energy:

$$\Psi = \Psi^b + \Psi^f \tag{1}$$

For the dissipative fracture energy Ψ^f the use of the explicit definition that involves integration over the crack surface $\Gamma(t)$ can be numerically costly. Instead, in the phase-field approach an equivalent expression that involves calculation of the energy as a domain integral is used, given as [6]:

$$\Psi^f = \int_\Gamma G_c \, d\Gamma \approx \int_V G_c \gamma(\phi, \nabla\phi) dV \tag{2}$$

where the critical energy release rate G_c is a material parameter. The crack density function is expressed as $\gamma(\phi, \nabla\phi) = \frac{1}{C_w}\left(\frac{w(\phi)}{l} + l|\nabla\phi|^2\right)$ [1]. For the case of brittle fracture the commonly used values in literature are $w(\phi) = \phi^2$ and $C_w = 2$. The continuous damage state variable, $\phi \in [0, 1]$, describes the scalar damage field ranging smoothly between the broken ($\phi = 1$) and the intact ($\phi = 0$) material state [6]. The length scale parameter l is used to control the width of the crack approximation zone.

The fracture energy can then be computed as:

$$\Psi^f = \int_V \frac{G_c}{2l}(\phi^2 + l^2|\nabla\phi|^2) dV \tag{3}$$

The bulk energy can be expressed as:

$$\Psi^b = \int_{V/\Gamma} \psi(\phi, \epsilon) \, dV = \int_V [g(\phi) \, \psi(\epsilon)^{e+} \; + \; \psi(\epsilon)^{e-}] dV \tag{4}$$

where the degradation function is selected for this problem as $g(\phi) = (1-\phi)^2$, and it is used to account the loss of stiffness that the fracture cause in the material. The bulk energy is also splitted into a compressive ($\psi(\epsilon)^{e-}$) and tensional ($g(\phi) \, \psi(\epsilon)^{e+}$) part in order to resolve the unrealistic symmetric behaviour in terms of crack propagation in both tension and compression. For this project the degradation function will always be applied to the elastic bulk modulus. This means that the model will only be valid for loads in tension. For the case of elastic material response the strain energy per unit volume of the intact material is described by: $\psi(\phi, \boldsymbol{\epsilon}) = g(\phi) \, \psi(\boldsymbol{\epsilon})^e = g(\phi) \, \frac{1}{2} \boldsymbol{\epsilon} \; \boldsymbol{D} \; \boldsymbol{\epsilon}$.

Therefore for this project, the total internal energy can be summarized as:

$$\Psi = \int_V (1-\phi)^2 \psi^e(\boldsymbol{\epsilon}) dV + \int_V \frac{G_c}{2l}(\phi^2 + l^2 |\nabla\phi|^2) dV \tag{5}$$

Defining the energy functional $\Pi = \Psi - W^{ext}$, the external work follows as:

$$W^{ext} = \int_V \bar{\boldsymbol{b}}\, \boldsymbol{u}\, dV + \int_\Gamma \bar{\boldsymbol{t}}\, \boldsymbol{u}\, d\Gamma \tag{6}$$

where $\bar{\boldsymbol{b}}$ and $\bar{\boldsymbol{t}}$ are the prescribed volume and boundary force vectors respectively. According to the principle of minimum total potential energy, the equilibrium state is taking place when the potential energy Π reaches a minimum.

For minimization of the energy functional, partial derivatives of the terms are calculated with respect to the field variables:

$$\begin{aligned}
\delta\Psi &= \frac{\partial \Psi}{\partial \boldsymbol{\epsilon}} \delta\boldsymbol{\epsilon} + \frac{\partial \Psi}{\partial \phi} \delta\phi \\
&= \int_V g(\phi) \frac{\partial \psi^e(\boldsymbol{\epsilon})}{\partial \boldsymbol{\epsilon}} \delta\boldsymbol{\epsilon}\, dV + \int_V \left[\frac{\partial g(\phi)}{\partial \phi} \psi^e(\boldsymbol{\epsilon}) + \frac{G_c}{2l} \frac{\partial \gamma(\phi, \nabla\phi)}{\partial \phi} \right] \delta\phi\, dV \\
&= \int_V \boldsymbol{\sigma}\ \delta\boldsymbol{\epsilon}\, dV + \int_V \frac{\partial g(\phi)}{\partial \phi} \psi^e(\boldsymbol{\epsilon})\, \delta\phi\, dV + \int_V \frac{G_c}{2l} \frac{\partial \gamma(\phi, \nabla\phi)}{\partial \phi}\, \delta\phi\, dV
\end{aligned}$$

where the constitutive equation for an elastic material model describes the stress tensor as:

$$\boldsymbol{\sigma} = g(\phi) \frac{\partial \psi^e(\boldsymbol{\epsilon})}{\partial \boldsymbol{\epsilon}} = (1-\phi)^2 \boldsymbol{D}\ \epsilon \tag{7}$$

for the material stiffness tensor $\boldsymbol{D}$ given for a 2-D field. Implementing the small strain setting as $\boldsymbol{\epsilon} = \frac{1}{2}[\nabla \otimes \boldsymbol{u} + \nabla \otimes \boldsymbol{u}]$, and by using the Gauss Divergence theorem as well as the definition of the traction stress vector $\boldsymbol{t} = \boldsymbol{\sigma}\, \boldsymbol{n}$, the equation can be written as:

$$\delta\Psi = -\int_V [\boldsymbol{\sigma}\, \nabla]\, \delta\boldsymbol{u}\, dV + \int_\Gamma \boldsymbol{t}\, \delta\boldsymbol{u}\, d\Gamma + \int_V [-2(1-\phi)\psi^e(\boldsymbol{\epsilon}) + \frac{G_c}{l}(\phi - l^2\Delta\phi)]\, \delta\phi dV + G_c\, l \int_\Gamma \nabla\phi\, \boldsymbol{n}\, \delta\phi\, d\Gamma$$

where the symbol $\Delta = \nabla \cdot \nabla$ is used. The corresponding partial derivative of the virtual external work follows as:

$$\delta W^{ext} = \int_V \bar{\boldsymbol{b}}\, \delta\boldsymbol{u}\, dV + \int_\Gamma \bar{\boldsymbol{t}}\, \delta\boldsymbol{u}\, d\Gamma$$

Hence, the minimization of the energy functional $\delta\Pi = 0$ lead to $\delta\Psi - \delta W^{ext} = 0$ which make it possible to identify the governing equations for the final strong form as:

$$\begin{cases}
\nabla\boldsymbol{\sigma} + \bar{\boldsymbol{b}} = 0\ in\ V & (8) \\
\boldsymbol{t} = \bar{\boldsymbol{t}}\ on\ \Gamma_{\bar{t}} & (9) \\
\boldsymbol{u} = \bar{\boldsymbol{u}}\ on\ \Gamma_{\bar{u}} & (10) \\
-2(1-\phi)\, \psi^e(\boldsymbol{\epsilon}) + \dfrac{G_c}{l}\, (\phi - l^2\Delta\phi)\ =\ 0\ in\ V & (11) \\
\nabla\phi \cdot \boldsymbol{n} = 0\ on\ \Gamma & (12)
\end{cases}$$

Introducing the crack driving state function $\tilde{D} = \frac{\psi^e(\boldsymbol{\epsilon})}{\frac{G_c}{2l}}$, Eq.(11) can be expressed as:

$$-l^2\Delta\phi + (1+\tilde{D})\, \phi = \tilde{D}\ in\ V \tag{13}$$

For a qualitative study of the crack propagation $\frac{G_c}{2l}$ can be set equals to 1. This is an simplification for the implementation in this project which works while developing the code for crack prediction, but has to be considered when comparing with experimental data in a quantitative study. In order to prevent the nonphysical crack healing phenomenon after the load is removed, the history field variable is introduced as:

$$H(t) := \max_{\tau=[0,t]} \tilde{D}(\tau) \tag{14}$$

and it can be used to equivalently express the above equation as:

$$-l^2 \Delta\phi + (1+H)\phi = H \; in \; V \tag{15}$$

2.1.2 Weak form

In order to numerically solve the problem, the weak formulation of the governing equations needs to be performed. The displacement field equilibrium Eq.(8) is integrated over the volume and multiplied with a kinematically admissible virtual displacement $\delta\boldsymbol{u}$:

$$-\int_V (\boldsymbol{\sigma}\,\nabla)\,\delta\boldsymbol{u}\,dV = \int_V \bar{\boldsymbol{b}}\,\delta\boldsymbol{u}\,dV \tag{16}$$

Using the Gauss divergence theorem, the Cauchy's stress theorem, $\boldsymbol{t} = \boldsymbol{\sigma}\,\boldsymbol{n}$, and taking into account that $\delta\boldsymbol{\epsilon} = \nabla\,\delta\boldsymbol{u}$, we get the weak form of the displacement field as:

$$\int_V \boldsymbol{\sigma}\;\delta\boldsymbol{\epsilon}\,dV = \int_V \bar{\boldsymbol{b}}\,\delta\boldsymbol{u}\,dV + \int_\Gamma \bar{\boldsymbol{t}}\,\delta\boldsymbol{u}\,d\Gamma \tag{17}$$

For the derivation of the weak form of the damage field equilibrium Eq.(11) is integrated over the volume of and multiplied with an virtual damage $\delta\phi$. The final form of the expression is:

$$\int_V \left[\frac{G_c}{l}\phi - 2(1-\phi)\psi^e(\boldsymbol{\epsilon})\right]\,\delta\phi\,dV + \int_V G_c\,l\,\nabla\phi\,\nabla\delta\phi\,dV = 0 \tag{18}$$

with boundary condition $\nabla\phi\cdot\boldsymbol{n} = 0$. Using the history field variable, the above equation can be written as:

$$\int_V [((1+H)\phi - H)\,\delta\phi + l^2\,\nabla\phi\,\nabla\delta\phi]\,dV = 0 \tag{19}$$

2.1.3 FE form

In order to derive the FE form, the weak form equation need to be expressed in Voigt format. For a 2-D problem, the displacement and strain terms with corresponding virtual components can be formulated as [3]:

$$\boldsymbol{u}(x,y) = \begin{bmatrix} u_x(x,y) \\ u_y(x,y) \end{bmatrix}, \quad \delta\boldsymbol{u}(x,y) = \begin{bmatrix} \delta u_x(x,y) \\ \delta u_y(x,y) \end{bmatrix}$$

$$\boldsymbol{\epsilon}(x,y) = \nabla\boldsymbol{u}(x,y) = \begin{bmatrix} \epsilon_{xx}(x,y) \\ \epsilon_{yy}(x,y) \\ \gamma_{xy}(x,y) \end{bmatrix}, \quad \delta\boldsymbol{\epsilon}(x,y) = \nabla\delta\boldsymbol{u}(x,y) = \begin{bmatrix} \delta\epsilon_{xx}(x,y) \\ \delta\epsilon_{yy}(x,y) \\ \delta\gamma_{xy}(x,y) \end{bmatrix}$$

Using a finite element discretization, the field variables are expressed as:

$$\boldsymbol{u}(x,y) = \sum_{k=1}^{n} N_k^u(x,y) \begin{bmatrix} u_{x,k} \\ u_{y,k} \end{bmatrix} = \boldsymbol{N}^u\,\boldsymbol{a}^u \tag{20}$$

with

$$\boldsymbol{N}^u = \begin{bmatrix} N_1^u(x,y) & 0 & ... & N_n^u(x,y) & 0 \\ 0 & N_1^u(x,y) & ... & 0 & N_n^u(x,y) \end{bmatrix}, \quad \boldsymbol{a}^u = \begin{bmatrix} u_{x,1} \\ u_{y,1} \\ . \\ . \\ . \\ u_{y,k} \end{bmatrix}$$

For the small strain definition it is:

$$\boldsymbol{\epsilon} = \nabla \boldsymbol{u} = \nabla \boldsymbol{N}^u \, \boldsymbol{a}^u = \boldsymbol{B}^u \, \boldsymbol{a}^u$$

with

$$\boldsymbol{B}^u = \begin{bmatrix} \frac{\partial {N_1}^u(x,y)}{\partial x} & 0 & \frac{\partial {N_2}^u(x,y)}{\partial x} & 0 & ... & \frac{\partial {N_n}^u(x,y)}{\partial x} & 0 \\ 0 & \frac{\partial {N_1}^u(x,y)}{\partial y} & 0 & \frac{\partial {N_2}^u(x,y)}{\partial y} & ... & 0 & \frac{\partial {N_n}^u(x,y)}{\partial y} \\ \frac{\partial {N_1}^u(x,y)}{\partial y} & \frac{\partial {N_1}^u(x,y)}{\partial x} & \frac{\partial {N_2}^u(x,y)}{\partial y} & \frac{\partial {N_2}^u(x,y)}{\partial x} & ... & \frac{\partial {N_n}^u(x,y)}{\partial y} & \frac{\partial {N_n}^u(x,y)}{\partial x} \end{bmatrix}$$

The discretization of the damage field is described as:

$$\phi(x,y) = \sum_{k=1}^{n} N_k^\phi(x,y) \, \phi_k = \boldsymbol{N}^\phi \boldsymbol{a}^\phi \tag{21}$$

where

$$\boldsymbol{N}^\phi = \begin{bmatrix} N_1^\phi(x,y) & N_2^\phi(x,y) & ... & N_n^\phi(x,y) \end{bmatrix}, \quad \boldsymbol{a}^\phi = \begin{bmatrix} \phi_1 \\ \phi_2 \\ . \\ . \\ . \\ \phi_k \end{bmatrix}$$

The derivative of the damage variable is approximated as

$$\nabla \phi(x,y) = \nabla \boldsymbol{N}^\phi \, \boldsymbol{a}^\phi = \boldsymbol{B}^\phi \boldsymbol{a}^\phi \tag{22}$$

where

$$\boldsymbol{B}^\phi = \begin{bmatrix} \frac{\partial {N_1}^\phi(x,y)}{\partial x} & \frac{\partial {N_2}^\phi(x,y)}{\partial x} & ... & \frac{\partial {N_n}^\phi(x,y)}{\partial x} \\ \frac{\partial {N_1}^\phi(x,y)}{\partial y} & \frac{\partial {N_2}^\phi(x,y)}{\partial y} & ... & \frac{\partial {N_n}^\phi(x,y)}{\partial y} \end{bmatrix} \tag{23}$$

By utilizing the Galerkin's method, the virtual components of the field variables can be described as

$$\delta \boldsymbol{u} = \boldsymbol{N}^u \delta \boldsymbol{c}^u \tag{24}$$

$$\delta \boldsymbol{\epsilon} = \boldsymbol{B}^u \delta \boldsymbol{c}^u \tag{25}$$

$$\delta \phi = \boldsymbol{N}^\phi \delta \boldsymbol{c}^\phi \tag{26}$$

$$\delta \nabla \phi = \boldsymbol{B}^\phi \delta \boldsymbol{c}^\phi \tag{27}$$

with arbitrary coefficient vectors $\delta \boldsymbol{c}^u$ and $\delta \boldsymbol{c}^\phi$. Inserting the approximation of the displacement and damage variables together with their virtual counterparts into the weak form equations $\delta W^{int} - \delta W^{ext} = 0$, we obtain the relation from Eq.(17) as:

$$\delta {\boldsymbol{c}^u}^T \left(\int_V {\boldsymbol{B}^u}^T \boldsymbol{\sigma} dV \; - \; \int_V {\boldsymbol{N}^u}^T \bar{\boldsymbol{b}} \, dV \; - \; \int_\Gamma {\boldsymbol{N}^u}^T \bar{\boldsymbol{t}} \, d\Gamma \right) \; = \; 0$$

$$\Rightarrow \delta \boldsymbol{c}^{u^T} \left(\boldsymbol{F}^{int,u} - \boldsymbol{F}^{ext,u}\right) = 0 \Rightarrow \boldsymbol{F}^{int,u} = \boldsymbol{F}^{ext,u}$$

for the force vectors for the displacement field to be given as:

$$\boldsymbol{F}^{int,u} = \int_V \boldsymbol{B}^{u^T} \boldsymbol{\sigma} dV \tag{28}$$

$$\boldsymbol{F}^{ext,u} = \int_V \boldsymbol{N}^{u^T} \bar{\boldsymbol{b}}\, dV + \int_\Gamma \boldsymbol{N}^{u^T} \bar{\boldsymbol{t}}\, d\Gamma \tag{29}$$

In a similar manner, the derivations for Eq.(19) result to

$$\delta \boldsymbol{c}^{\phi^T} \left(\int_V \{[(1+H)\, \boldsymbol{N}^\phi\, \boldsymbol{a}^\phi - H]\, \boldsymbol{N}^\phi + l^2\, \boldsymbol{B}^{\phi^T}\, \boldsymbol{B}^\phi\, \boldsymbol{a}^\phi\}\, dV \right) = 0$$

$$\Rightarrow \delta \boldsymbol{c}^{\phi^T} \left(\boldsymbol{F}^{int,\phi} - \boldsymbol{F}^{ext,\phi}\right) = 0 \Rightarrow \boldsymbol{F}^{int,\phi} = \boldsymbol{F}^{ext,\phi}$$

for the internal force vectors for the damage field to be given as:

$$\boldsymbol{F}^{int,\phi} = \int_V \{[(1+H)\, \boldsymbol{N}^\phi\, \boldsymbol{a}^\phi - H]\, \boldsymbol{N}^\phi + l^2\, \boldsymbol{B}^{\phi^T}\, \boldsymbol{B}^\phi\, \boldsymbol{a}^\phi\}\, dV \tag{30}$$

and , due to displacement condition

$$\boldsymbol{F}^{ext,\phi} = 0$$

where $H = max(^{n-1}H, \psi^e)$ at a current time step n .

Concluding, the system of equations can be written with the following manner in order to be solved in an iterative manner using the Newton-Raphson method:

$$\begin{bmatrix} \boldsymbol{K_{uu}} & \boldsymbol{K_{u\phi}} \\ \boldsymbol{K_{\phi u}} & \boldsymbol{K_{\phi\phi}} \end{bmatrix} \begin{bmatrix} \Delta \boldsymbol{a}^u \\ \Delta \boldsymbol{a}^\phi \end{bmatrix} = \begin{bmatrix} \boldsymbol{F}^{ext,u} \\ \boldsymbol{F}^{ext,\phi} \end{bmatrix} - \begin{bmatrix} \boldsymbol{F}^{int,u} \\ \boldsymbol{F}^{int,\phi} \end{bmatrix} \tag{31}$$

where

$$\boldsymbol{K_{uu}} = \frac{\partial \boldsymbol{F}^{int,u}}{\partial \boldsymbol{a}^u} = (1-\phi)^2 \int_V \boldsymbol{B}^{u^T}\, \boldsymbol{D}\, \boldsymbol{B}^u\, dV \tag{32}$$

$$\boldsymbol{K_{u\phi}} = \frac{\partial \boldsymbol{F}^{int,u}}{\partial \boldsymbol{a}^\phi} = -2(1-\phi) \int_V \boldsymbol{B}^{u^T}\, \boldsymbol{D}\, \boldsymbol{B}^u\, \boldsymbol{N}^\phi\, dV \tag{33}$$

$$\boldsymbol{K_{\phi u}} = \frac{\partial \boldsymbol{F}^{int,\phi}}{\partial \boldsymbol{a}^u} = -2(1-\phi) \int_V \boldsymbol{N}^{\phi^T}\, \boldsymbol{D}\, \boldsymbol{B}^u\, \boldsymbol{B}^u\, dV \tag{34}$$

$$\boldsymbol{K_{\phi\phi}} = \frac{\partial \boldsymbol{F}^{int,\phi}}{\partial \boldsymbol{a}^\phi} = \int_V [l^2\, \boldsymbol{B}^{\phi^T}\, \boldsymbol{B}^\phi + (1+H)\, \boldsymbol{N}^\phi\, \boldsymbol{N}^\phi]\, dV \tag{35}$$

2.2 Fatigue extension

The theory of phase-field modeling described in the previous chapter is able to predict the crack initiation and propagation with some features for loads in the low cycle regime or monotonic loading. This since the crack driving state function and the splitting of the bulk energy into a compressive and tensile part prevents the material from acting nonphysical in terms of healing or driving the crack propagation in compression. What the model is unable to consider however, is the reproduction of crack initiation nor crack growth for cyclic loads with amplitudes below the fracture limit in brittle materials [6]. This section will extend the model with fatigue considerations for brittle fracture, corresponding to the high-cycle fatigue regime.

Aiming to implement the fracture energy degradation due to the repeated externally applied loads, the accumulated strain energy $\bar{\psi}(t)$ is introduced. Specifically, the physical result is the crack

propagation to take place as the number of loading cycles is increased, which is equivalent to the degradation of the material fracture properties during the cyclic loading. In order to achieve this the structural loading history needs to be taken into account. Considering the case of high-cycle fatigue where the externally applied load is below the plastic limit, the bulk energy ψ^e follows a periodical function according to the external applied loading. That is because by its definition ψ^e is dependent on the strain $\boldsymbol{\epsilon}$. For this reason, the variable $\bar{\psi}$ is used as a local measure of repeated deformation energy changes during the loading history.

It is important to notice that in order to utilize $\bar{\psi}$ in a generalized phase-field fatigue formulation model, it needs to be defined in a manner that the monotonic loading case is not affected. To satisfy this condition, in this project the $\bar{\psi}$ is computed at each Gauss Point of the finite element model as described by the equation:

$$\frac{\partial \bar{\psi}}{\partial t} \; = \; - \, \langle - \frac{\partial \psi^e}{\partial t} \rangle \tag{36}$$

This definition denotes that $\bar{\psi}$ is increased only during the unloading phases, thus not affecting the loading phases. Therefore the accumulated strain energy is considered as the sum of negative differences of total deformation energy during the cyclic loading [6].

In addition, a fatigue degradation function $\hat{F}(\bar{\psi}) \; \in \; [0, 1]$ is introduced as:

$$\hat{F}(\bar{\psi}) \; = \; e^{-\alpha \bar{\psi}} \tag{37}$$

where $\hat{F}(\bar{\psi} = 0) \; = \; 1$, $\hat{F}(\bar{\psi} \rightarrow \infty) \; = \; 0$ and $\frac{d\hat{F}}{dt}(0 < \bar{\psi} < \infty) \leq 0$, while α is a selected constant value.

Therefore, the history variable that is used to describe the phase-field fatigue model is given as:

$$H(t) := \max_{[\tau < t]} \frac{\psi^e(\tau)}{\hat{F}(\bar{\psi}(\tau))} \tag{38}$$

Proceeding to the solution of the fatigue problem, the finite element formulation is performed and the system of equations is defined as in Eq.(31). The stiffness matrices K_{uu} , $K_{u\phi}$ and $K_{\phi\phi}$ are defined as in Eq.(32), Eq.(33) and Eq.(35) respectively, while due to the implemented definition of the history variable the stiffness matrix $K_{\phi u}$ is given as:

$$\boldsymbol{K_{\phi u}} \; = \; -2(1 - \phi) \int_V \boldsymbol{N}^{\phi^T} \, \frac{\partial H}{\partial \boldsymbol{\epsilon}} \, \boldsymbol{B}^u \, dV \tag{39}$$

where at a particular time step n :

$$\frac{\partial H}{\partial \boldsymbol{\epsilon}} \; = \begin{cases} 0 & \text{if} \quad \frac{\psi^e(\boldsymbol{\epsilon})}{\hat{F}({}^n\bar{\psi})} \; < \; {}^{n-1}H \\ \frac{\frac{\partial \psi^e}{\partial \boldsymbol{\epsilon}}}{\hat{F}({}^n\bar{\psi})} \; - \; \frac{\psi^e}{\hat{F}({}^n\bar{\psi})^2} \, \frac{\partial \hat{F}({}^n\bar{\psi})}{\partial \bar{\psi}} \, \frac{\partial \bar{\psi}}{\partial \boldsymbol{\epsilon}} & \text{if} \quad \frac{\psi^e(\boldsymbol{\epsilon})}{\hat{F}({}^n\bar{\psi})} \; \geq \; {}^{n-1}H \end{cases} \tag{40}$$

with

$$\frac{\partial \bar{\psi}}{\partial \boldsymbol{\epsilon}} \; = \begin{cases} 0 & \text{if} \quad {}^{n-1}\psi^e \; - \; {}^n\psi^e < 0 \\ - \, \frac{\partial \psi^e}{\partial \boldsymbol{\epsilon}} & \text{if} \quad {}^{n-1}\psi^e \; - \; {}^n\psi^e \geq 0 \end{cases} \tag{41}$$

3 Method

In this chapter, the methodology for the project is presented. The first part consists of an investigation of fracture patterns for monotonic loading in both Matlab and Comsol. Next, the procedure of applying a cyclic load to the monotonic case in order to analyze the behaviour is described. The final part of the method chapter covers necessary modifications and completions for implementing fatigue on the phase-field model, which both includes the already provided geometry and also an attempt on a new geometry. The final part of the chapter concerns the verification process of comparing the model with analytical data and assessing its plausibility.

3.1 Investigation of fracture pattern for monotonic loading

In this section an investigation of the fracture pattern for a linearly increasing load on the specimen will be made. The main reason for this simulation was to verify that the phase-field model is working before proceeding. It was made both in Matlab and Comsol to be able to compare if there are any numerical differences using the different softwares.

3.1.1 Monotonic loading in Matlab

Before any fatigue loads are considered it was of interest to have a model describing the fracture pattern for monotonic loading. For this, an open-source Matlab code from an earlier project was provided by one of the teaching assistants. The code is using phase-field modeling for monotonic loading in pure tensile (mode I) or shear (mode II) conditions. The geometry of the specimen is quadratic with a side length of 1mm with clamped boundary conditions at the bottom boundary and applied load at upper boundary. The fracture pattern for pure tensile testing shown in Figure (1), and the corresponding load versus displacement curve can be shown in Figure (2). The code is considered when the specimen is fully damaged and terminates when a full fracture appears. In Figure (2), it can be noted that the crack starts to grow when the internal force is starting to decrease which corresponds to displacements above $u = 0.0055mm$. The full fracture displacement can be read as $u = 0.005612mm$. In Figure (3) the crack pattern for a time step between the initial crack and final failure can be viewed.

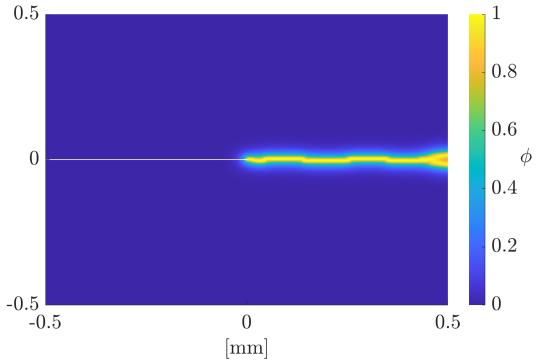

Figure 1: Crack pattern at final failure visualized in terms of the damage variable ϕ for monotonic tensile test.

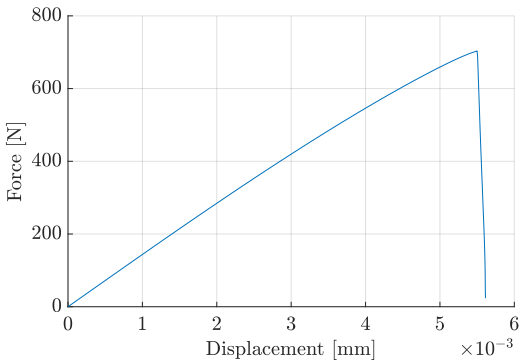

Figure 2: Load/displacement curve until final failure.

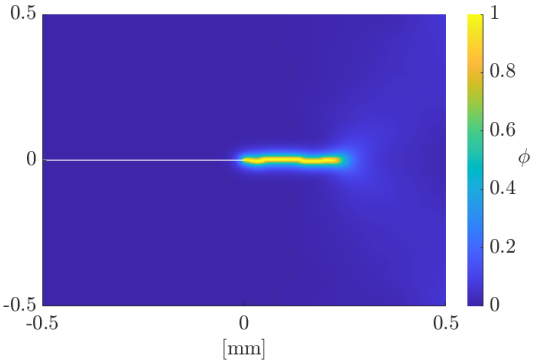

Figure 3: Crack pattern for monotonic loading for displacement $u_y = 0.005556mm$.

3.1.2 Monotonic loading in Comsol

The COMSOL Multi-physics platform was utilized to implement the phase field approach, which enables the simulation of mathematical and physical problems by incorporating application-specific modules. This makes it well-suited for multi-field modeling. Within the COMSOL module, the variables and equations were defined, allowing for the investigation of multiple conditions and cases using the solver and post-processing capabilities.

The model comprises three primary modules: Solid Mechanics, History strain module, and Phase Field Module. These modules are discretized using the standard Finite Element Discretization. The Phase Field Module is dedicated to the representation of the phase field variable ϕ, achieved by modifying a module governed by the Helmholtz equation. The History strain variable **H** and the Distributed ODEs and DAEs Interfaces are employed in the construction of the History-strain Module, wherein the History strain variable is not directly solved. Instead, a "previous solution" solver is used to record results from previous time steps and obtain the field H [8][9].

The Solid Mechanics module relies on the linear elastic material library and focuses initially on describing fracture patterns under monotonic loading. A preexisting COMSOL model from a previous project by one of the Ph.D. students was adopted, utilizing a Staggered solver.

This study employed a specific model, featuring a single-edge-notched square with dimensions $x = 1 \times 10^{-3}$m and $y = 1 \times 10^{-3}$m. Assuming plane strain conditions, the length scale parameter was set to $l_0 = 1.2 \times 10^{-5}$m. The entire domain was discretized with 7942 domain elements (3-node triangular) and 388 boundary elements. The maximum element size was 0.005mm in the domain with crack growth and 0.037mm in the remaining domain.

The phase-field modeling of both pure tensile (mode-I) and pure shear loading conditions was tested using the models. The fracture patterns resulting from pure tensile loading are illustrated in the figures. These patterns were obtained by applying displacement-controlled loading at the upper boundary.

Figure (5) depicts the relationship between the force acting in the y-direction and displacement during tensile loading. Notably, a significant drop in load-carrying capacity is observed after a displacement of 5x10^{-3}mm, indicating the occurrence of material failure, specifically the initiation of a crack.

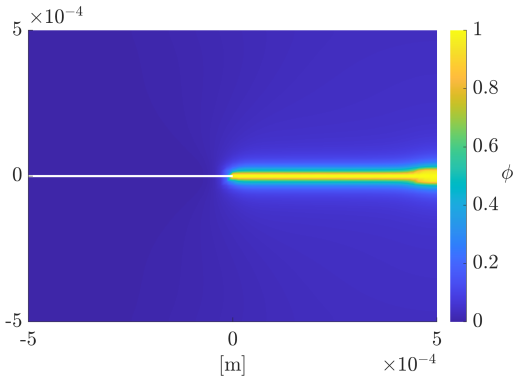

Figure 4: Crack pattern visualisation in terms of damage variable ϕ for monotonic tensile loading.

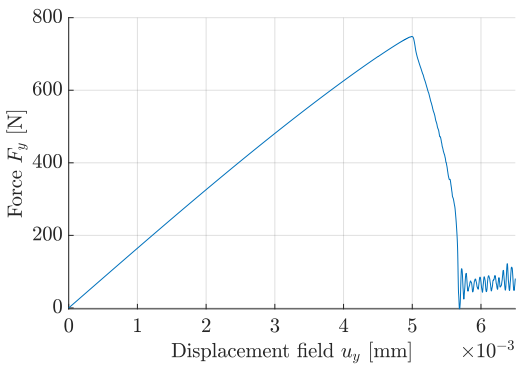

Figure 5: Reaction Force v/s Displacement [y] graph for tensile loading.

3.2 Cyclic loading adjustments

As the project will investigate the feasibility of solving fatigue problems using phase-field modeling, the next step was to implement a simple cyclic loading for the problem to be able to analyze the response of the damage. In the first subsection, the loading will be restricted according to what the implemented model is able to handle. In the next section, a history variable is introduced for the model to be able to store damage that has progressed in earlier loading cycles.

3.2.1 Cyclic loading in Matlab

The internal energy of the domain can be described as Eq. (5) which follows as:

$$\Psi = \int_V (1-\phi)^2 \psi^e(\epsilon) dV + \int_V \frac{G_c}{2l}(\phi^2 + l^2 |\nabla \phi|^2) dV$$

For this project the split of the bulk energy is not being considered in the implementation and the fracture degradation function will always be applied. This means that the model will not be able to simulate cyclic tensile-compressive loads as in Figure (6). Instead, the load will be implemented as positive pulsating as in Figure (7). Since fatigue is damaged over a long duration of time, it is crucial to have a load amplitude that is lower than the critical monotonic fracture load in order to hold for many loading cycles. The chosen peak value of the cyclic load is selected to be $u_y = 0.005556mm$ since it was a displacement where a crack pattern before full failure could be detected in the monotonic loading case according to Figure (2). In order to capture the short displacement range $(0.0055_y \leq 0.005612)$ [mm] where the crack propagation is taking place, the step size needed to be adopted with a finer step size for the displacement magnitudes in this region. This was made by arranging the time steps with a ratio where a larger amount of time steps were located at the top peaks.

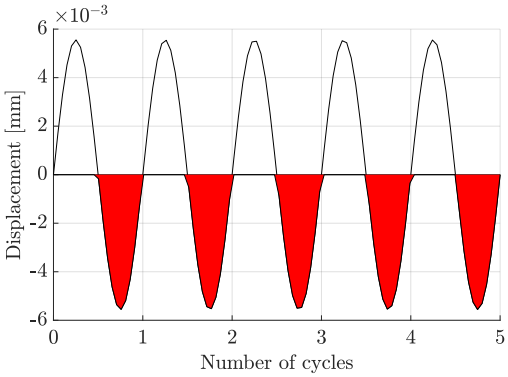

Figure 6: Visualization of tensile-compression load. The red area is loading in compression which the implemented model is not able to handle.

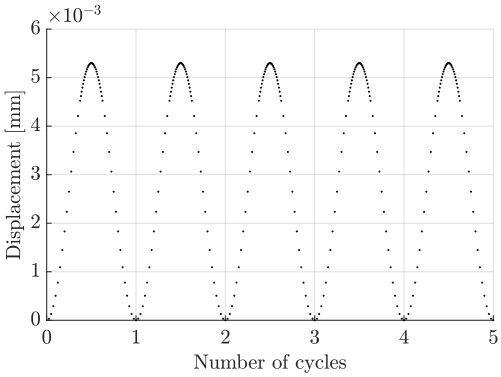

Figure 7: Load is incremented in terms of displacement control over time with adaptive step size at loading peaks. The peak value of the displacement is $u_y = 0.005556mm$.

When applying load according to Figure (7) the crack should look the same as for the monotonic case, Figure (3), after the loading cycles if no fatigue phenomena are implemented. Instead, the material appears to be fully intact. The reason for this is that the material at this moment is "healing" in a nonphysical sense every time the loading is decreased. In order to capture the crack growth from earlier loading cycles a history variable had to be implemented. In the case of monotonic increasing loading this variable is unnecessary since the previous time step is the most critical one. However, for cyclic loading, it is needed to prevent healing of the crack during unloading. The history variable was introduced in the strong formulation, Eq. (15), which follows as:

$$H(t) := max_{\tau=[0,t]} \tilde{D}(\tau)$$

With the history variable implemented the most critical loading state will always be stored as the crack driving state. The resulting crack pattern after five cycles is presented in Figure (8). A visualization of the development of $H(t)$ as the sum over all elements can also be shown in Figure (9). Comparing the crack length with the monotonic case, Figure (1), it can be noted that the cracks are almost of the same length which should be the case. However, it can always be some differences depending on the convergence of the solution.

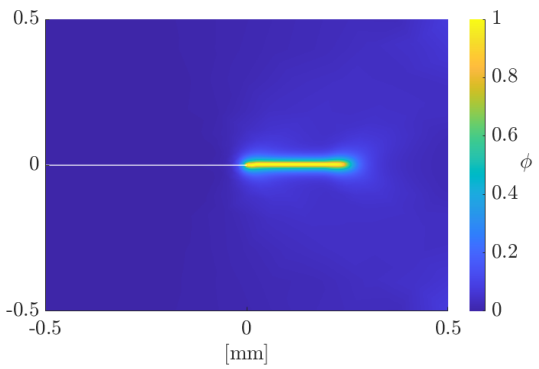

Figure 8: Crack pattern after 5 cycles with history variable implemented.

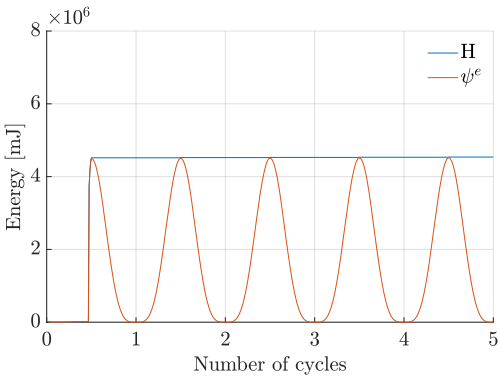

Figure 9: Development of history variable, H.

3.2.2 Cyclic loading in Comsol

In COMSOL, cyclic loading was implemented similarly to Matlab to simulate the model's behaviour. The applied load followed a positive pulsating pattern, with a critical displacement of 5.1 x 10^{-3}mm considered as the threshold for complete failure and crack growth. As fatigue damage occurs gradually over an extended period, this displacement value was chosen as the amplitude for the cyclic loading.

To generate the cyclic displacement required, a sine wave waveform was generated and combined with the displacement. This waveform, resembling the one used in Matlab, accounted for the cyclic loading in COMSOL. Additionally, a history variable was introduced to prevent healing, mirroring the methodology employed in the Matlab code. In order to conduct a detailed analysis of crack growth, a series of experiments were performed with various displacement amplitudes. The Figure (10) and Figure(11) provided showcases an example waveform and illustrates the resulting crack growth.

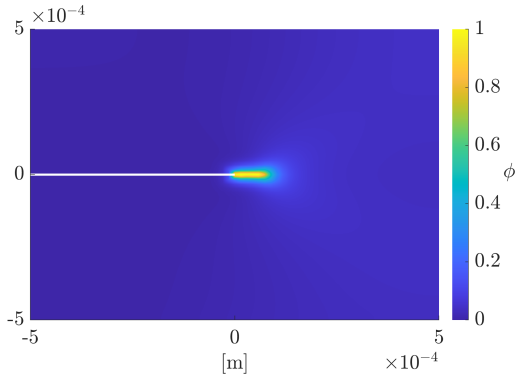

Figure 10: Crack pattern visualisation in terms of damage variable ϕ for cyclic loading. The amplitude of the displacement is u_y=0.0058mm.

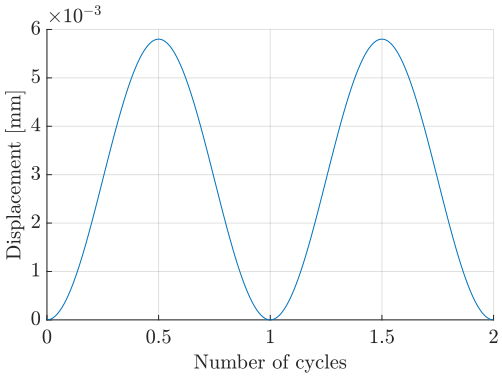

Figure 11: Visualization of how the load is incremented in terms of displacement control over time. The amplitude of the displacement is u_y = 0.0058mm.

3.3 Fatigue implementation

In this chapter, the methodology of the fatigue implementation is introduced. First, the implementation process on the already provided model is described in both Matlab and Comsol. Next, the method for producing a new model that is comparable to existing experiments is presented, followed by a description of the fatigue implementation attempts in Matlab and Comsol.

3.3.1 Fatigue implementation on provided model

The first step of the fatigue implementation process was to apply it to the provided model on which the monotonic tests were carried out on. This was done both in Matlab and Comsol in order to verify the implementations and the behaviors of the cracks according to theory.

Matlab

In order to make the fatigue adjustments in Matlab in line with the theory presented in section 2.2, the fatigue degradation function needed to be implemented. An approximation of the function

was made in the form of an exponentially decreasing function from 1 to 0 as $\hat{F}(\overline{\psi}) = e^{-\alpha\overline{\psi}}$ (Eq. (37). The local accumulated energy in each step and element $\overline{\psi}(t)$ was hence first implemented such that it only increases if the gradient of the bulk energy in the current time step is negative. Equation (42) below describes this relation and originates from Eq. (36):

$$^{n}\overline{\psi} =^{n-1} \overline{\psi} + \langle^{n-1}\psi^{e} -^{n} \psi^{e}\rangle \tag{42}$$

The next step was to adjust the history variable according to Eq. (38), which in Matlab corresponds to the following formulation for each element and time step:

$$H(t) = max(\frac{^{n}\psi^{e}}{\hat{F}(\overline{\psi})},^{n-1} H) \tag{43}$$

In order to visualize the results from the fatigue adjustments and thus behavior of the crack, the history variable H, the accumulated energy $\bar{\psi}$ and the bulk energy ψ^{e} was plotted as a sum of all element contributions in each time step. The first check of the fatigue code was to set α to zero, which should result in the same plots as for the monotonic cyclic tests since it forces $\hat{F}$ to be one. This assumption aligned with the results. Then different combinations of prescribed displacement amplitudes, time steps, loading cycles, and constant values for the fatigue degradation parameter α were tested in order to obtain a visible crack with a slow crack propagation representative of real-life fatigue behavior. As a result, it became apparent that a very low value of α was necessary for the solution to convergence, along with a large number of time steps in order to resolve the damage field properly in each cycle peak as for the monotonic cyclic case.

In this test α was set to 0.00001, the displacement amplitude as $0.0026mm$ and 10 cycles during 200 steps. Figure (12) illustrates the crack pattern with these parameters. The crack plot shows a formation of a crack, and after visualizing it in the software Paraview, a slight crack propagation after the first cycle producing a crack could be seen in each following cycle.

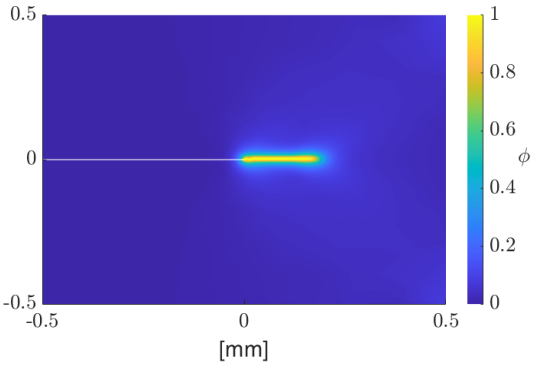

Figure 12: Crack pattern after 10 cycles.

Figure (13) below shows the element sum of the history variable, the accumulated energy, and the strain energy, during each loading cycle. Figure (14) furthermore shows the fatigue degradation function in one element during each cycle, in order to visualize its behavior. Figure (13) shows similar behavior in the strain energy as for the monotonic, which is expected. Furthermore, it is clear that the accumulated energy increases in each cycle where the strain energy decreases, in accordance with the expected results (see Eq. (42)). The history variable increases rapidly to a high magnitude, which is expected when considering the sum of all elements. The fatigue degradation function decreases stepwise as it should, and since only a small number of cycles were studied with a very small α value, the exponentially decreasing curve is approaching a linear curve instead.

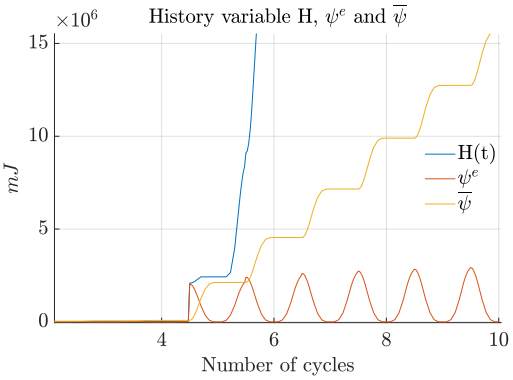

Figure 13: Element summation of H, ψ^e and $\overline{\psi}$.

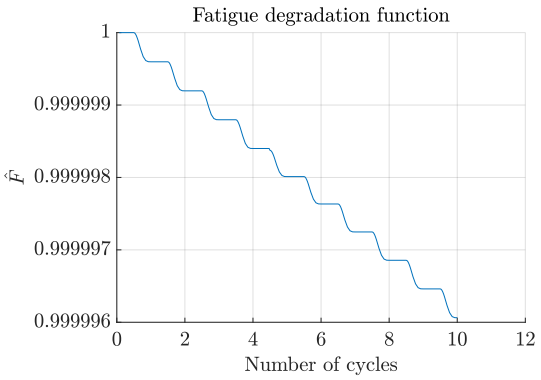

Figure 14: Fatigue degradation function in one element.

After the verification of the fatigue implementation was completed, the parameters were adjusted for a simulation over a larger amount of cycles, and with a higher resolution in order to mimic a real-life fatigue situation as closely as possible. Even though the adapted step size improved the resolution at the peaks for the previous parameters, it had to be further refined at the crucial loading peaks. This became especially apparent during the cycle in which the crack first appeared, where the previous test would cause the crack to grow to a certain length instantly without any intermediate steps. In addition, the number of steps and cycles was increased largely for a more accurate representation of reality. The plots were also adjusted by instead plotting each variable at different points along the crack path over all cycles, in order to more clearly visualize the variables connected to crack growth. Hence, the damage variable ϕ was also plotted.

Comsol

The fatigue implementation in the current model involved incorporating a degradation function, denoted as $\hat{F}(\overline{\psi})$, inspired by similar approaches used in Matlab. To expedite the process, an updated version of the model was utilized, leveraging Constitutive relations and State Variables. The weak form equation was adjusted by introducing $\hat{F}(\overline{\psi})$ according to equation 37.

In the COMSOL state variable framework, we defined the history variable and accumulated strain energy as functions of time (s), which were continuously updated by the time-dependent solver. This approach acted as a "previous solution" solver, considering time derivatives and boundary conditions to obtain the History variable (H) and accumulated strain energy ($\overline{\psi}$).

Throughout the model setup, multiple iterations were performed, varying the α values for $\hat{F}$. Through this iterative process, it was observed that higher α values resulted in faster model divergence. After careful consideration, an optimal value of 0.000001 was determined for α. However, this choice significantly increased computational time. To validate the equations and boundary conditions, an iterative verification process was implemented. This process revealed the inherent complexities of the model, stemming from the geometry, variable relationships, and time constraints. Despite these challenges, the model produced partial results that were comparable to those obtained using Matlab. Unfortunately, due to the prolonged computational time, the model did not converge, preventing the attainment of the desired solutions.

3.3.2 Fatigue implementation on new model

In order to achieve the goal of a qualitative assessment and calibration of the developed fatigue implementation, an attempt on creating a new geometry with existing results to compare with was

made. A compact tension specimen in pure mode 1 loading with similar geometry to the previous one with an initial notch, and with fatigue test results was obtained from [2]. Thus, a new mesh was created in Comsol that fulfilled the dimension constraints according to [2]. The mesh was created with the same element type and the same boundary conditions, whereby it was inserted into the existing fatigue code. However, after trying many different combinations of time steps, number of cycles, displacement amplitudes, and α, no reasonable results were obtained from the model. Some issues that were faced were no crack growth at all, a fully cracked plate and no convergence in the time stepping, leading to unphysically large values on ψ and hence causing the solution to diverge. Another attempt to solve the problem was made by implementing a force controlled load insetad of the displacement control. This however still led to solution begin unable to converge. The same issues were apparent when trying to simulate with Matlab as in Comsol, which led to the conclusion of redirecting the focus of the project towards the old geometry and loading case.

3.4 Matlab FEM model verification using analytical methods

Since our finite element model developed in Matlab is based on a number of assumptions and uncertainties related to domain discretizations, mathematical shape functions and solution procedures, the evaluation of the model's performance should take place for verification purposes. For the fatigue problem that is studied analytical methods are available in the literature. Hence, a correlation between the numerical and analytical approach is performed so as to examine the agreement between the two methods.

As a first approach, the stress intensity factor K_I is calculated as a measure of severity of a crack situation affected by the length of crack a, stress and geometry, as

$$\Delta K_I = K_{I,max} - K_{I,min} = F\,(\sigma_{max} - \sigma_{min})\,\sqrt{\pi\, a} \tag{44}$$

where for our problem $\sigma_{min} = 0$, since the component is loaded in tensile and the unloading is taking place to the original state. The factor F depends on the geometry of the component as a function of the fraction of the crack length to the width of the component b. For the initial crack, it is $a_{initial}/b = 0.5$, hence the value $F = 1.12$ could be used according to the literature.

According to Paris' law, for a stable macroscopic crack growth the criterion that should be fulfilled is:

$$K_I < K_{IC} \tag{45}$$

where the fracture toughness K_{IC} is a material parameter. Since our developed numerical model is not calibrated based on real material data, the value for the fracture toughness is selected according to the literature for a typical ferritic-pearlitic steel, as $K_{IC} = 66\, MPa\sqrt{m}$ [2] .

The developed model describes the fatigue in region of medium crack growth rates, corresponding to the straight line in the log-log fit of Region II in Paris' law curve. The linear part of the curve describes the growth rate of the length of the crack with respect to the number of cycles as:

$$\frac{da}{dN} = C\,(\Delta K_I)^m \tag{46}$$

with the parameter F assumed to be constant in Eq.(44) for ΔK_I. Integrating Eq.(46), the computation of the amount of cycles needed for a crack of length a_i to grow to a length a_f can be performed as:

$$\Delta N = N_f - N_i = \frac{a_f^{(1-\frac{m}{2})} - a_i^{(1-\frac{m}{2})}}{C\,(F\,\Delta\sigma\,\sqrt{\pi})^m\,(1-\frac{m}{2})} \tag{47}$$

where material parameters used for a ferritic-perlitic steel under Mode I loading and $\sigma_{min} = 0$ case are [2] :

$$C = 6.89 \cdot 10^{-12}\,\frac{m/cycle}{(MPa\,\sqrt{m})^m} \quad with \quad m = 3$$

4 Result

In this chapter the results of the implemented phase-field models for fatigue problems are presented. The subsections will view results from the implementations in Matlab with graphs including earlier introduced variables. Finally the comparison of the results with analytical data is presented.

4.1 Simulation of pulsating tensile fatigue problem in Matlab

The final run of the phase-field model with extended fatigue considerations were made as a positive pulsating tensile test on a geometry with unit lengths in millimeters according to Figure (15). For the simulation the constant parameter α was selected to $1e^{-5}$ as input to the fatigue degradation function, in order to not make the crack grow too fast in each cycle. The number of cycles were selected to be 100 which with the considered time discretization of 60 time steps per cycle corresponds to 6000 time steps. Also, the displacement for the applied Dirichlet boundary condition on the upper boundary, was chosen to be below the critical crack driving peak values in order to not make the crack propagate already at the first loading cycle. The chosen displacement amplitude was $u_y = 0.0026mm$.

In Figure (15) and Figure (16) the progression of the crack pattern after five and 100 cycles respectively can be shown including some reference points used for analyzing the data. The selected points are within the region where the crack is propagating and are at the following coordinates: $A = [0.15, 0]$, $B = [0.20, 0]$ and $C = [0.25, 0]$. In Figure (17) a more detailed view can be shown of the development of the field variable ϕ for the three specified points. It can be noted that during the first 4 cycles no crack is propagating. Instead stress concentrations at the initial notch tip is accumulated. First at cycle 5 the material at the top of the initial notch is fully damaged. From Figure (17) it can also be shown that it takes approximately 30 cycles for the crack to grow from point A to B, while it takes around 40 cycles between B and C. This mean that the crack growth is slowing down the longer the simulation is running. This can also be seen by looking at the slopes for the three different curves of the damage variable.

In Figure (18) and Figure (19) the history variable and strain energy are viewed. The strain energy and hence also the history variable are decreasing in magnitude further in along the crack. As presented in Eq. (37) the accumulated energy shown in Figure (20) has a large influence on $\hat{F}$ which hence is an important variable to connect cyclic loads with fatigue problems.

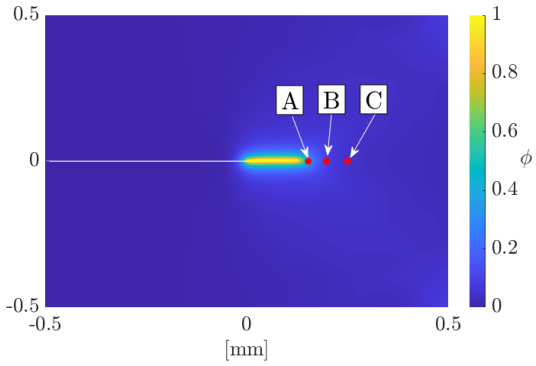

Figure 15: Crack pattern for the considered geometry after 5 cycles. Coordinates A=[0.15,0], B=[0.20,0] and C=[0.25,0] specified for comparison in later graphs.

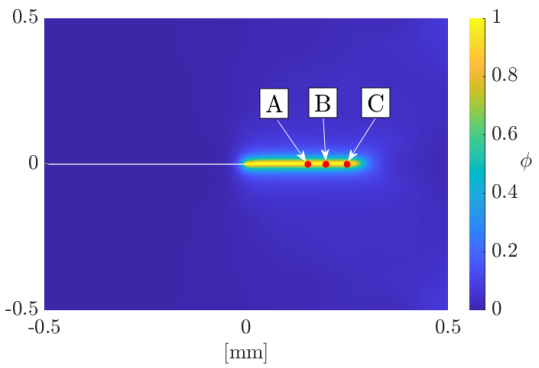

Figure 16: Crack pattern after 100 cycles.

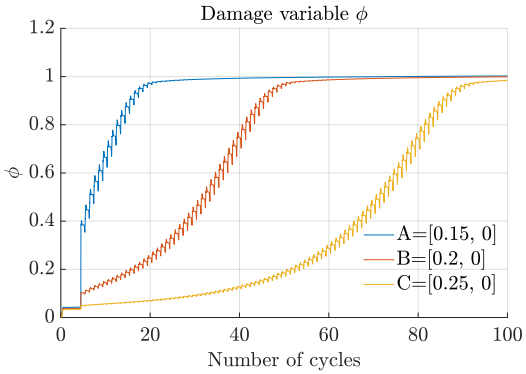

Figure 17: Development of the damage variable ϕ at three different points.

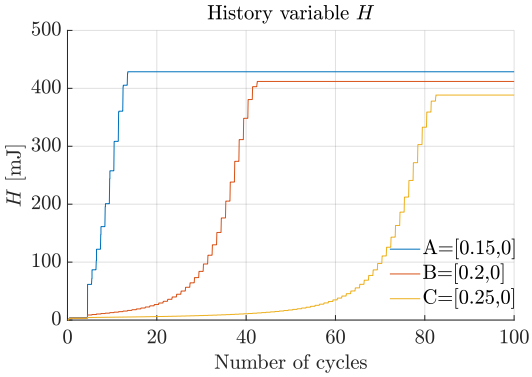

Figure 18: Development of the history variable, H.

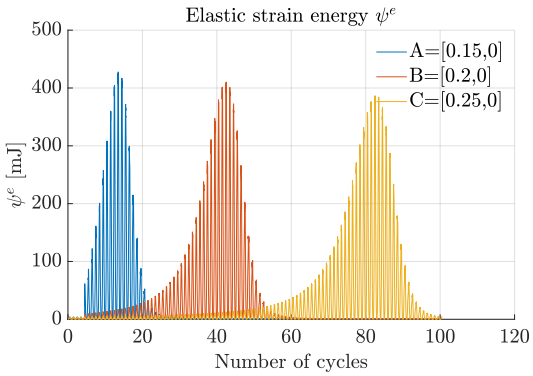

Figure 19: Development of elastic strain energy, ψ.

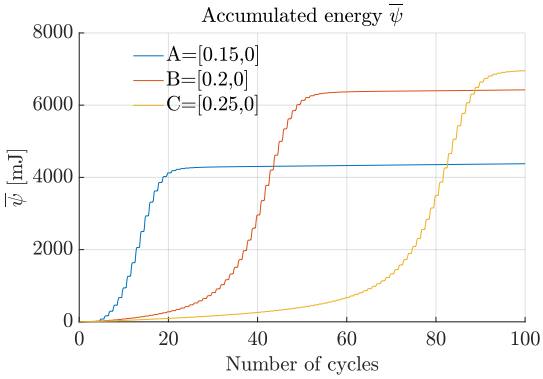

Figure 20: Development of accumulated energy, $\bar{\psi}$.

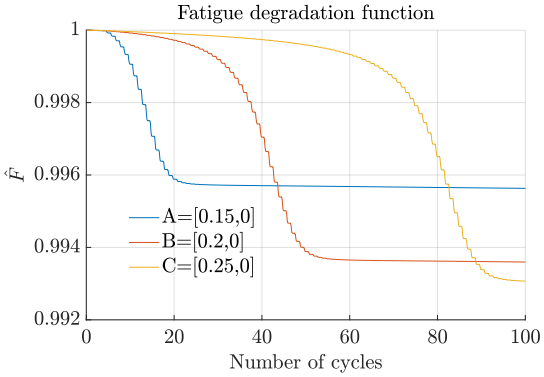

Figure 21: Development of the fatigue degradation function, $\hat{F}$.

4.2 Verification of Matlab model results with analytical solutions

The verification process described in section 3.4 can be followed in order to compare the Matlab results with the results from analytical solutions.

Specifically, verification tests took place for the selected loading cycles $N = 0,\ 5,\ 10$ and 20. For each cycle the length of the crack was measured. Since the displacement-controlled approach is used in the developed Matlab problem, the maximum stress at the top boundary was calculated during the post-processing phase. In particular, the maximum stress of the elements of the top edge of the component was averaged so as to be computed at each loading cycle. Then, using these Matlab data, Eq.(44) and Eq.(46) were utilized to compute the stress intensity factor at each cycle as well as the number of cycles needed for the crack to propagate from the previous length to the current one. The data from Matlab N, a and σ_{max} as well as the analytical results for K_I and ΔN are shown in Table 1.

N	a (mm)	$\sigma_{max}\,(MPa)$	$K_I\,(MPa\sqrt{m})$	ΔN
0	0.5	1393.36	61.85	-
5	0.64	732.91	36.81	76
15	0.66	645	32.89	23
20	0.675	528	27.23	79

Table 1: Parameters for verification of Matlab results according to analytical solutions

By observing the results, the fulfilment of criterion in Eq.(45) is achieved for all the analytically computed values of the stress intensity factor. On the other hand, the predicted number of cycles ΔN that the analytical derivations results is significantly higher than the applied loading in Matlab that result to this crack growth.

The differences between the analytical and Matlab results are mainly due to the selected modeling parameters. First, the parameter F was considered to be constant and equal to the value 1.12 that corresponds to the initial crack length. That value was used for all the calculations, while in reality the parameter F is increased as the length of the crack is increased. Moreover, parameters that are used in Matlab code as the α constant in Eq.(37) are not calibrated. Hence, the Matlab result of having important crack growth in only a few cycles is considered nonphysical while the analytical solutions ΔN are more close to reality.

5 Discussion

In this section the obtained results are first discussed and analyzed, followed by an assessment of the initial goals in terms of whether or not they were achieved. Finally, possibilities of future work on fatigue implementation on phase-field modelling is presented and discussed.

5.1 Analysis of results

The result presented in the previous chapter is showing crack propagation for loads in 100 cycles. The results are reasonable in terms of how the presented variables are connected to each other, and how they together make the crack propagate in each cycle. Firstly, it can be seen in Figure (15) that point A is placed at the crack propagation of five cycles, which was the first crack appearance for the chosen parameters. This aligns well with the presented variables in Figure (17) - (21), where the blue curve starts to form at around five cycles as well. An increase in the damage variable, the history variable, strain energy and accumulated energy is observed, which is reasonable considering the theory presented in Chapter 2 for the crack driving variables. The fatigue degradation function is simultaneously decreasing, caused by the degradation of the material that mimics fatigue fracture propagation. For all three points along the crack path, the same reasoning can be applied. Furthermore, it can be seen in Figures (19) and (18) that the strain energy and hence also the history variable is decreasing in magnitude further along the crack. This is due to the fact that the material has been degraded by the fatigue degradation function $\hat{F}$, that for the three points is developing according to Figure (21). For a continued crack growth over a larger amount of cycles this phenomenon would continue until final material degradation and final fracture, occurs.

Another noticeable behaviour is that the first crack which occurs at around five cycles, develops rapidly to a relatively long crack. This could be observed in a software, Paraview, which is an aid for visualizing the crack growth over the time period. This can however also be seen in Figure (17) when looking at the damage variable, where the blue curve increases significantly in just one cycle in the beginning. This is most likely due to the accumulated stress concentrations from the first four cycles. Moreover, the crack propagation seems to slow down the further the crack grows. This can for instance be seen from the damage variable in Figure (17), where the slope is far steeper at point A than at point C. One reason for this could be that the phase-field model is implemented with displacement control, meaning that the applied load is represented by a Dirichlet boundary condition. As the material weakens due to the fracture growth from the fatigue implementation, the crack driving energy will also decrease as could be seen in Figure (19). Consequently, the displacement amplitude would have to be increased over time in order to compensate for the material degradation, with the purpose of maintaining the crack growth over a larger amount of cycles.

5.2 Achievement and assessment of initial goals

By revisiting the initial goals in Chapter 1.2, the work can be evaluated and assessed with the aim of providing a solid foundation for future work. Since the goals were determined at an early stage of the project, which is partly a research project due to its relatively new concept of fatigue phase-field modelling, some of the goals were not achieved as intended. Since a finite element code for phase-field modelling was provided for a monotonic loading case, a new code was not developed from scratch. Instead, the main focus was to extend the model to include a fatigue implementation, which was one of the initial goals. In the process, many different tests concerning the plausibility of each step in the implementation were made.

Redirecting the focus and aim of the project was necessary in order to produce results that are

valuable for further investigation within the field. For instance, neither calibration nor validation with experiments was conducted mainly due to time limitations for the project. These limitations also led to issues in applying the fatigue phase-field model on a new geometry, which in turn means that the model at this stage is not suitable for usage in real-life applications. Furthermore, a larger number of cycles would have to be simulated in order to mimic real-life fatigue problems. This includes calibration of the fatigue degradation function and the parameter α, which could be calibrated using, for example, Eq. (47). Although the expression in Eq. (47) is analytical, it is very well established in fatigue theory and rooted in experiments.

The final goal for the project was to qualitatively assess the ease and feasibility of the fatigue implementation of phase-field models. The assessment is based on experiences during the project, with benefits complemented by recognized difficulties. As mentioned in Chapter 1, there are many numerical benefits to phase-field modelling for fractures in general, such as reduced computational effort in not explicitly modelling the crack, and the ability to simulate complex crack problems.

Many of the faced difficulties for the fatigue implementation concerned convergence in the Newton solver at certain time steps. One of the main convergence difficulties was with the time step. The sensitivity to time step size was especially crucial at the most critical crack-driving displacements, namely the loading peaks. The need for extensive time step adjustments was a significant realization, which helps refine the resolution at the loading peaks and hence increases the possibility for convergence. Another noticeable difficulty was that the simulations were time-consuming, particularly when increasing the number of steps at the peaks. This affected the ease of parameter calibration such as obtaining an α that mimics real-life fatigue that only causes crack propagation after a large number of cycles. Additionally, many of the difficulties were realized after a lot of testing. One example is the issue with displacement control causing the crack to slowly stagnate when simulating a large amount of cycles. Another late realization was that the solver used from the original code in monotonic loading was unsuitable for cyclic loading. It was a version of a Newton solver that utilized a form of extrapolation, which led to issues in the implementation of the history variable. To summarize, the ease of using phase-field modelling on fatigue problems will most likely be more evident in time when research projects like this increase. The most time-consuming part is realizing the difficulties and limitations of the models, which is usually the case in the early stages of research fields.

5.3 Future work

Given the produced results of this project and the assessment of the work above, it is clear that there are great possibilities for future work within phase-field modelling for fatigue problems. Even though the work needs to be complemented with calibrations and validations, the discoveries along the way as well as the result aligning well with the principle of fatigue crack growth has the potential to be a foundation for further work. A summary of the focus points of future work will be presented here.

As mentioned in the previous chapter the crack seems to slow down the longer the crack grows due to displacement control. For further investigation of crack growth, an implementation of force control could solve this problem. For force control the stress, due to the applied load, will be constant for each cycle which leads to a more constant crack growth over time. Also, most theories and analytical expressions on fatigue problems are based on force-controlled tests, meaning that the calibration and validation procedure would benefit from a force-control approach. The next step after this implementation would hence be to run the simulation over a much larger amount of loading cycles, in order to simulate high cycle fatigue as in real life. Consequently, the amplitude of the force, in this case, would need to be decreased accordingly. Thereafter the fatigue degradation function and its parameter α can be calibrated, followed by validation tests from comparing the

simulation with experiments. If the degradation function proves unsuitable due to its simplicity, a more complex function can also be created in order to achieve better accuracy of the model. Recommendations for the degradation function can be found in previous research and in literature.

Another clear point of improvement is the computational time of the model. This is of course the contradiction to the simultaneous problem of time step-dependent resolution at the loading peaks. However, the adaptive step size method itself has room for improvement. A possible approach could be to optimize the time stepping in a way that only increases the number of steps at the very locations where it is essential. The adaptive method developed in this project was approximate and established from observed behavior rather than assessing the necessity based on the numerical results in each step.

An additional possibility for improvement is further development of the Comsol model. Using the load-controlled approach, the Comsol model could first be validated using results from experiments. Then, the validated Comsol model could be used for verification of the developed MATLAB code. A parameter that is suggested to be examined in the verification process is the crack length growth with respect to the number of cycles. In addition, both the COMSOL and MATLAB models could be verified using analytical derivations according to the literature.

Finally, some notes regarding the constitutive modelling assumptions are worth mentioning for future work. The theory that the implementation is based on is assuming a linear elastic response of the material. This means that when simulating a real-life problem it is important to do an estimation before simulating, in order to assess if the input data conditions are valid for high-cycle fatigue problems. These considerations haven't been taken into account in this project due to time limitations, and are important remarks when proceeding to simulate for a large number of cycles.

6 Conclusion

In conclusion, the produced results align well with the theoretical outcomes for phase-modelling of fatigue, considering the modelling limitations described in chapter 5.2. Some difficulties were however discovered as the project progressed, such as displacement control leading to a stagnating crack propagation, extensive computational time when experimenting and convergence issues due to sensitivity to time stepping and loading parameters. Consequently, some initial goals mainly regarding calibration and validation, were left unfulfilled due to time limitations. In order to proceed on developing the phase-field model for fatigue fracture, implementing force control is recommended due to the more reasonable crack growth over time as well as the increased accuracy in calibration and validation of the model. Additionally, developing the Comsol fatigue model further would solidify the verification process of the implementations in Matlab. Regarding the feasibility of fatigue extensions to phase-field models, the implementation process has proven to be time consuming mostly due to the model's sensitivity to convergence related parameters. However, with additional research along with the results obtained from this project, fatigue implementations on phase-field models has the potential to make prominent progress and thus facilitate less computationally expensive simulations for more complex fatigue fracture problems.

References

[1] Ritukesh Bharali, Fredrik Larsson, and Ralf Jänicke. "Computational homogenisation of phase-field fracture". In: *European Journal of Mechanics - A/Solids* 88 (2021), pp. 11–17. ISSN: 0997-7538. DOI: https://doi.org/10.1016/j.euromechsol.2021.104247. URL: https://www.sciencedirect.com/science/article/pii/S0997753821000346.

[2] Norman E.Dowling. *Mechanical behavior of materials: engineering methods for deformation, fracture, and fatigue*. 2013, pp. 334–415. ISBN: 9780273782568.

[3] N.S. Ottosen and H. Petersson. *Introduction to the Finite Element Method*. Report TVSM. 1990, pp. 292–310. URL: https://books.google.se/books?id=I8KDtwAACAAJ.

[4] Christoph Schreiber et al. "A phase field modeling approach of cyclic fatigue crack growth". In: *International Journal of Fracture* 225 (2020), pp. 89–100. DOI: https://doi.org/10.1007/s10704-020-00468-w. URL: https://link.springer.com/article/10.1007/s10704-020-00468-w?utm_source=getftr&utm_medium=getftr&utm_campaign=getftr_pilot.

[5] Martha Seiler et al. "An efficient phase-field model for fatigue fracture in ductile materials". In: *Engineering Fracture Mechanics* 224 (2020), p. 106807. ISSN: 0013-7944. DOI: https://doi.org/10.1016/j.engfracmech.2019.106807. URL: https://www.sciencedirect.com/science/article/pii/S0013794419303200.

[6] Karlo Seleš et al. "A general phase-field model for fatigue failure in brittle and ductile solids". In: *Computational Mechanics* 67 (2021), pp. 1431–1432. DOI: https://doi.org/10.1007/s00466-021-01996-5.

[7] Sikang Yan, Christoph Schreiber, and Ralf Müller. "An efficient implementation of a phase field model for fatigue crack growth". In: *International Journal of Fracture* 237 (2022), pp. 47–60. DOI: https://doi.org/10.1007/s10704-022-00628-0. URL: https://link.springer.com/article/10.1007/s10704-022-00628-0?utm_source=getftr&utm_medium=getftr&utm_campaign=getftr_pilot#citeas.

[8] Shuwei Zhou, Timon Rabczuk, and Xiaoying Zhuang. "Phase field modeling of quasi-static and dynamic crack propagation: COMSOL implementation and case studies". In: *Advances in Engineering Software* 122 (2018), pp. 31–49. ISSN: 0965-9978. DOI: https://doi.org/10.1016/j.advengsoft.2018.03.012. URL: https://www.sciencedirect.com/science/article/pii/S0965997818300061.

[9] Shuwei Zhou et al. "Phase field modelling of crack propagation, branching and coalescence in rocks". In: *Theoretical and Applied Fracture Mechanics* 96 (2018), pp. 174–192. ISSN: 0167-8442. DOI: https://doi.org/10.1016/j.tafmec.2018.04.011. URL: https://www.sciencedirect.com/science/article/pii/S016784421830123X.